© JETIR.ORG | ISSN: 2349-5162 | ESTD Year : 2014 | Monthly Issue

JOURNAL OF EMERGING TECHNOLOGIES AND INNOVATIVE RESEARCH (JETIR)

An International Scholarly Open Access, Peer-reviewed, Refereed Journal

Aero Vision Net: A Deep Learning-Powered Framework for Aerial Image Restoration with Advanced Digital Enhancement Techniques

[1] Rejeena K.A , [2] Smitha. K ,

[1]Assistant Professor in dept of Electronics, MES College Marampally ,[2]Assistant Professor in dept of Industrial Instrumentation and Automation ,MES College Marampally

Abstract

Aerial image restoration plays a major role in applications such as urban planning, environmental monitoring, and disaster management, where high-quality imagery is crucial for accurate decision-making. However, aerial images often suffer from challenges like noise, poor contrast, color distortion, and atmospheric interference, which hinder effective analysis. Traditional restoration techniques struggle to address these multifaceted issues, particularly in complex scenarios. This study proposes an advanced approach integrating digital image processing techniques with deep learning, specifically using Cycle GAN (Cycle-Consistent Generative Adversarial Networks), to restore aerial images. The methodology begins with a comprehensive image restoration pipeline, including color stabilization, saturation enrichment, and contrast improvement, followed by deep learning (DL) enhancement through Cycle GAN. The restoration process is carried out on the USC-SIPI Image Database, focusing on aerial imagery. Key image characteristics such as saturation, contrast, and brightness are adjusted to enhance the clarity and usability of the images. The CycleGAN model, operating on unpaired datasets, enables effective translation from low-quality to high-quality images, preserving essential features and improving visual appeal. Evaluation metrics, including Structural Similarity Index (SSIM), Peak Signal-to-Noise Ratio (PSNR), and Mean Absolute Error (MAE), were employed to assess the performance. The proposed model attained a PSNR of 38.34, an SSIM of 0.9806, and an MAE of 0.005, demonstrating superior restoration quality compared to existing methods. These results highlight the model's capability to improve image quality while conserving critical facts. The CycleGAN-based approach provides a powerful and adaptable solution for real-world aerial image restoration, offering significant improvements over traditional techniques and making it a valuable tool for applications requiring high-fidelity image analysis.

Keywords: *Aerial Image Restoration, Deep Learning, Digital Image Processing, Color Stabilization, Contrast Enhancement, Image Quality Improvement*.

1.Introduction

Aerial image restoration enhances the clarity and detail of satellite and drone imagery, enabling more precise analysis for tasks like land use mapping, wildlife conservation, and assessing the impacts of natural disasters [1].High-quality aerial imagery is essential for accurate analysis, interpretation, and decision-making. However, aerial images are often degraded due to various factors such as atmospheric distortions, sensor noise, motion blur, and lighting inconsistencies [2]. This degradation can significantly impact the usability of the images for downstream applications, demanding effective restoration methods. Traditional image restoration methods handle classical digital image processing methods, such as deblurring algorithms, histogram equalization, and de noising filters. While these approaches have proven effective in some scenarios, they often struggle to handle the complexity of degradation in aerial images, which can involve simultaneous challenges such as noise, poor contrast, and color instability [3]. Furthermore, environmental factors like haze, fog, and varying sunlight intensities add additional layers of complexity to the restoration process. Addressing these challenges requires sophisticated algorithms capable of enhancing the visual quality of aerial images while preserving critical details.

Among the challenges in aerial image restoration, noise and poor contrast are the most common issues. Noise, caused by sensor inaccuracies or transmission errors, reduces the clarity of images, making it difficult to extract meaningful information. Similarly, poor contrast, often due to uneven lighting or atmospheric interference, obscures features within the image, complicating tasks such as object detection and segmentation. Another significant challenge is color distortion, where the hues in an image appear unnatural due to imbalances in the RGB channels [4]. These issues underscore the limitations of traditional restoration methods in handling the multifaceted nature of degradation in aerial imagery.

Digital image processing has emerged as a foundational tool for addressing these challenges [5]. Techniques like color stabilization, saturation enrichment, and contrast improvement form the basis for enhancing degraded images. Color stabilization ensures that images maintain a natural appearance by balancing the RGB channels, while saturation enrichment enhances the vibrancy of colors, making details more discernible. Contrast improvement, on the other hand, sharpens the differences between light and dark regions, improving the visibility of fine details. Together, these techniques provide a comprehensive approach to initial restoration, setting the stage for more advanced enhancements.

In recent years, DL has revolutionized the field of image restoration. Unlike traditional methods, DL models can adapt to diverse scenarios, making them highly effective for aerial image restoration [6]. The integration of DL into the restoration pipeline enables a level of precision and adaptability that was previously unattainable. This research focuses on a hybrid approach to aerial image restoration, combining traditional digital image processing techniques with DL models. The major contributions of the study are:

- To develop an advanced image restoration pipeline combining traditional image processing techniques and DL models.
- To integrate color stabilization and saturation enhancement methods, ensuring more accurate color representation and improving the vibrancy and consistency of aerial images.
- To enhance contrast and brightness, improving feature visibility in aerial imagery.
- To utilize DL enhancement, enabling the translation of low-quality aerial images into high-quality counterparts while preserving important features and structures.
- To use comprehensive evaluation metrics, including PSNR, SSIM, MAE, and MSE, to assess the effectiveness of the suggested restoration method.

The paper is organized into five sections. Section 2 provides a comprehensive literature review, summarizing previous work on aerial image restoration. In Section 3, the methodology is presented, describing the proposed image restoration pipeline, incorporating advanced image processing and DL techniques. Section 4 covers the results and discussion, where the performance of the proposed methodology is analysed and compared to existing techniques. Finally, Section 5 offers a conclusion, summarizing the study's contributions.

1. Literature Review

Chenet al. [7] aimed to improve Wiener filtering de convolution for scattering image restoration by enhancing exposure doses and optimizing the K-value while also addressing noise through a neural network-based denoising model. The methodology involved an exposure-improved Wiener filtering technique with a denoising model that significantly enhanced PSNR and SSIM by 27.3% and 186.7%, respectively, on a dataset of speckle samples, achieving real-time recovery within 41.5 ms for five-megapixel resolution. However, the approach was limited in handling weak light scenes or complex patterns. Duttaet al. [8] explored image restoration tasks like denoising, super-resolution, and in painting by adapting quantum many-body physics principles into a DL framework. The methodology involved the development of a deep neural network, DIVA, based on the De-QuIP algorithm, which incorporated a quantum-inspired interaction layer and Hamiltonian operator for better image restoration. The model outperformed several state-of-the-art methods, achieving 97.43% SSIM and 37.42 dB PSNR on the Set5 dataset for super-resolution, but struggled with complex degradation tasks like Gaussian down sampling, where it did not match benchmark methods in quantitative performance.

Namet al. [9] proposed a method for age estimation from low-light facial images using a GAN (LAE-GAN) for image enhancement, followed by a CNN-based age estimation model. The proposed method achieved a PSNR of18.94, an SSIM of 0.6223, and an SNR of 1.3924. However, the study noted limitations such as incomplete restoration of high-frequency details like wrinkles and textures, additional noise, and increased processing time. Junget al. [10] employed an advanced U-net model grounded on local and global residual learning (RFSUNET) for

restoring images affected by multi-type noise, such as line noise, additive white Gaussian noise, and dark saturation. The model was evaluated using TIR and HS images, showing superior performance in noise removal and image restoration, with a PSNR of 32.89 and an SSIM of 0.9436. However, the study noted that CNN-based models, including RFSUNET, produced slightly blurry results compared to the ground truth images, highlighting a limitation in sharpness.

Zhao et al. [11] generated high-spatial multispectral images (MSIs) from low-cost natural color RGB (ncRGB) images for precision agriculture, focusing on maize and rice crops. The study used a DL-based MSI reconstruction method with a model (Model-NM) trained on ncRGB and MSI pairs, incorporating a combined loss function (MRAE loss and SID loss) to improve model robustness. The results demonstrated that the reconstructed MSIs provided superior NDVI values for differentiating irrigation treatments compared to RGB-derived TGI, although faced limitations in robust mapping functions. Kiruthika et al. [12] improved geospatial object detection in satellite images affected by noise and blur, proposing the deep Wiener de convolution denoising sparse auto encoder (DWDDSAE) model to enhance image quality. The study evaluated the model on the DOTA and NWPU VHR-10 datasets, achieving high accuracy (96.32%), edge similarity (86.88%), and notable improvements in PSNR (38.08 dB) and SSIM (0.883), outperforming existing methods in noise and blur removal.

Neheteet al. [13] enhanced degraded images affected by environmental factors such as haze, blur, fog, and rain using a two-stage architecture called FAPRNet. The model, utilizing a Fourier prior and a CNN-Transformer-based approach, separately refined the amplitude and phase information of degraded images, achieving superior performance across multiple restoration tasks like image deraining, dehazing, and low-light enhancement, using datasets such as NH-Haze, Dense-Haze, and RESIDE. The results showed significant improvements in PSNR and SSIM compared to existing methods; however, the model still exhibited computational overhead. Yuanet al. [14] enhanced the image restoration for CT images affected by blur and noise by integrating system blur and noise characterization with DL methods. The study presented two methods, input-variant and weight-variant, for incorporating auxiliary inputs into CNN architectures, demonstrating that the inclusion of these inputs significantly improved restoration performance. The results showed superior performance compared to baseline models, with higher PSNR values.

Guoet al. [15] introduced Mamba IR, an image restoration model that improves upon the Mamba model by incorporating local enhancement and channel attention to address issues like pixel forgetting and channel redundancy. The model was evaluated through extensive experiments on image super-resolution, showing improvements over SwinIR with similar computational costs, demonstrating its effectiveness in handling long-range dependencies with linear complexity. Yeet al. [16] proposed the refined transformer integrated with the convolutional block attention module (RT-CBAM) model, an advanced restoration method of underwater images according to a refined transformer architecture that improves the capture of both global and local features. The model incorporated a dilated transformer block, a global and local blind-patch network, and a multi-scale

convolutional block attention module, achieving superior results in detail recovery and color restoration compared to existing methods.

Despite significant advancements in image restoration techniques, several gaps remain unaddressed. Existing methods often struggle with complex degradation scenarios, such as weak lighting, high-frequency detail preservation, and intricate noise patterns. Techniques like Wiener filtering or DL-based approaches excel in specific tasks but face challenges in achieving generalizability across diverse applications, such as low-light enhancement, underwater image restoration, and geospatial analysis. Furthermore, many models exhibit computational overhead, limiting their real-time applicability for high-resolution images. While some methods incorporate advanced architectures like transformers and attention mechanisms, they still face trade-offs between sharpness, accuracy, and processing efficiency. These limitations highlight the need for robust, computationally efficient models that can handle diverse and complex degradations while maintaining high-quality restoration across various domains.

2. Materials and Methods

Aerial image restoration is crucial, where accurate and detailed imagery is indispensable. However, challenges like noise, poor contrast, and color distortion often degrade the quality of aerial images, making analysis and interpretation difficult. The integration of advanced digital image processing techniques with DL models offers a transformative solution, enabling precise and adaptive restoration. This combination ensures enhanced clarity, detail retention, and usability of aerial images, significantly improving their value for critical decision-making processes. Figure 1 illustrates the block diagram of the suggested model.

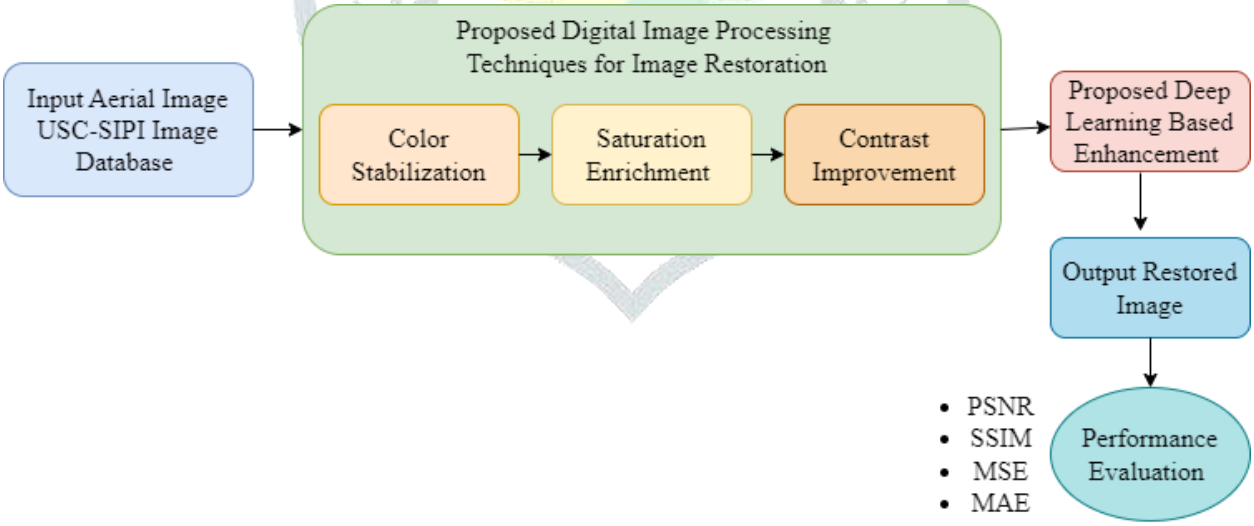

Figure 1. Proposed image restoration model

2.1 Dataset description

This study utilized the USC-SIPI Image Database from Kaggle, the public repository [17], which is a comprehensive collection of digitized images curated to advance studies in image processing, image analysis, and

machine vision. The database has expanded significantly, incorporating diverse images. It is structured into volumes, each representing a distinct category of images, with all files formatted as 8 bits/pixel for grayscale or 24 bits/pixel for color images. Image dimensions include sizes of $256 \times 256, 512 \times 512$, and 1024×1024 pixels, catering to a variety of research requirements.The USC-SIPI Image Database is organized into four main volumes, each developed for specific research needs. The textures volume includes Brodatz textures, texture mosaics, and their variations digitized at different rotations, making it ideal for studies in texture analysis and segmentation. The aerials volume features high-altitude imagery of locations like San Francisco, San Diego, and Earth from space, primarily supporting remote sensing and geospatial analysis. The miscellaneous volume contains iconic images such as the mandrill, peppers, and jellybeans, along with various everyday scenes, aiding general-purpose research in image recognition and enhancement. Lastly, the sequences volume comprises motion image sets, including moving heads, chemical plant flyovers, and toy vehicle movements, designed for motion tracking and dynamic scene analysis.

Images are stored in TIFF format for ease of access and compatibility, allowing researchers to work seamlessly across various platforms and software. As a cornerstone in the image processing research community, the USC-SIPI Image Database remains a critical resource. This study used the aerial images for effective processing. Figure 2 represents the sample aerial images from the dataset.

Figure 2. Sample images from the dataset

2.2 Proposed Digital Image Processing Techniques for Image Restoration

Aerial image restoration is critical for enhancing the usability of degraded images in applications like remote sensing, urban planning, and disaster response. Degraded images often suffer from poor contrast, color imbalances, and reduced saturation, limiting their interpretability and usefulness. The image processing pipeline addresses foundational image quality issues, providing essential corrections before DL-based enhancement.

2.2.1 Color Stabilization

Color stabilization is a technique used in image processing to correct color imbalances across the image, ensuring consistent color representation. The main goal is to adjust the RGB channels (Red, Green, Blue) such that the

overall image appears neutral in terms of color balance. This process compensates for various factors like lighting conditions or camera sensor discrepancies that could lead to color bias.A common approach to achieve this is based on the grey-world assumption, which states that in any natural scene, the average color of the scene should be neutral or grey. By assuming the average of all RGB intensities should be the same, the study computes adjustments to balance the channels accordingly. The input image $P(x, y)$ is typically represented as a set of three matrices, corresponding to the RGB channels. Each channel contains intensity values for every pixel (x, y) in the image, as in Equation 1.

$$P(x, y) = \{R(x, y), G(x, y), B(x, y)\} \quad (1)$$

where$R(x, y), G(x, y)$ and $B(x, y)$ are the intensities of the red, green, and blue components of the pixel at coordinates (x, y).The intensity values for each color channel range between 0 and 1, where 0 denotes no intensity and 1 shows maximum intensity.

The first step in color stabilization is calculating the mean brightness for each of the RGB channels. This is done by averaging the intensity values across all the pixels in the image for each channel .For each channel $c \in \{R, G, B\}$, the mean brightness μ_c is computed as in Equation 2.

$$\mu_c = \frac{1}{N}\sum_{x,y} P_c(x, y) \quad (2)$$

where $P_c(x, y)$represents the intensity of channel c at pixel $(x, y)$and N is the total number of pixels in the image.

To stabilize the colors, each channel is adjusted based on the relationship between its average brightness and the average brightness of the other channels. The adjustment is done using a logarithmic alignment as given in Equation 3.

$$P_c' = \left(\frac{\log(P_c)}{\log(\mu_c)}\right)^{\psi_c} \quad (3)$$

where P_c' is the adjusted intensity for channel c, ψ_c is an adjustment exponent that fine-tunes the channel alignment to avoid distortion and ensure the correction behaves well across different lighting conditions.The exponent ψ_c is a crucial parameter in this process. It controls the extent of the correction for each channel. This factor can be derived empirically or adjusted dynamically depending on the scene characteristics. If $\psi_c$is set too high or too low, the image can either be overcorrected or under corrected, leading to unnatural or poor color balance. After the channel alignment is applied, the adjusted RGB values P_R', P_G', and P_B', are recombined to form the final color-stabilized image $P'(x, y)$, which ensures that the color balance is consistent and closer to the grey-world assumption, as in Equation 4.

$$P'(x, y) = \{\{P_R'(x, y), P_G'(x, y), P_B'(x, y)\}\} \quad (4)$$

2.2.2 Saturation Enrichment

Saturation enrichment is an image processing technique aimed at improving the vibrancy of colors in an image. By enhancing the saturation, the colors in the image become more vivid, making the image appear livelier and aesthetically pleasing. Saturation is a measure of the intensity or vividness of a color. In color models like HSI (Hue, Saturation, Intensity) orHSV (Hue, Saturation, Value), the saturation component indicates how pure a color is, with higher saturation meaning more intense, vivid colors, and lower saturation corresponding to more muted, washed-out colors. Equation 5 mathematically defines Saturation S.

$$S = 1 - \frac{min(R,G,B)}{max(R,G,B)} \quad (5)$$

where$R, G,$ and B represent the red, green, and blue intensity values of a pixel.The saturation value ranges from 0 to 1 as in Equation 6.

$$S = \begin{cases} 0, \ represents\ a\ grayscale\ image \\ 1, \ represents\ maximum\ saturation \end{cases} \quad (6)$$

Before performing any further enhancement on the saturation, the process normalizes each of the RGB channels so that their values lie within the range [0, 1]. This normalization ensures consistency and facilitates subsequent adjustments. Equation 7 represents the normalized version of each channel P_c.

$$P_c' = \frac{P_c - min(P_c)}{max(P_c) - min(P_c)} \quad (7)$$

where $P_c$is the intensity of the channel (R, G, or B),$min(P_c)$and$max(P_c)$are the minimum and maximum intensity values of the channel, respectively. Saturation enrichment involves adjusting the minimum and maximum values of the RGB channels to increase the saturation. These adjustments aim to push the colors further from gray (neutral) and make them more vibrant. Two parameters are involved in these adjustments, ζ; the adjusted minimum value of the color channel and ψ; the adjusted maximum value of the color channel. Equation S 8 and 9 are the updates applied to ζ and ψ.

$$\zeta \leftarrow (1 - \lambda)\zeta \quad (8)$$

$$\psi \leftarrow \psi + (1 - \lambda) \quad (9)$$

where λ is a factor that controls the intensity of the adjustment. λ typically ranges from 0 to 1, where $\lambda = 0$ results in no change and $\lambda = 1$ applies the maximum possible adjustment.These adjustments expand the color range, increasing the difference between the minimum and maximum intensity values. This leads to more vivid colors as the saturation is increased.

Once the color channels have been adjusted, the next step is to further normalize the saturation values to ensure they fit within the desired range. This step makes sure that the enhanced saturation does not push the colors beyond the range of perceptible intensities. Equation 10 recalculates the saturation value Ω.

$$\Omega = \mu \cdot (\psi - \zeta) + \zeta (10)$$

where μ is a scaling factor employed to control the degree of saturation adjustment. Equation 11calculates the μ.

$$\mu = \frac{\psi - \zeta}{\Omega} (11)$$

The final output of the saturation enrichment process is an image where the colors are more vibrant and visually striking. By enhancing the saturation, the image appears more colorful, helping to emphasize the key features and details.Higher saturation values for pixels that are already colorful become more vivid. Reduced saturation for pixels that are already close to neutral or gray scale enhances the contrast between colorful and neutral areas.

2.2.3 Contrast Improvement

Contrast improvement is crucial for highlighting image features, making distinctions between objects or regions more pronounced. By using techniques like unsharp masking, it enhances local details and overall clarity. The initial step involves computing the brightness T as the average intensity across the R, G, B channels. This is expressed as in Equation 12.

$$T = \frac{1}{3} \sum_{C \in \{R,G,B\}} P_C \quad (12)$$

To emphasize details, edges in the image are extracted using a Laplacian kernel K. The Laplacian operator is effective in detecting areas of rapid intensity change, such as edges, by approximating the second derivative. The operation is performed via convolution as in Equation 13.

$$E = T \otimes K \ (13)$$

where E is the edge map,$\otimes$ denotes the convolution operation and K is typically an 8-connected kernel.

Once edges are detected, the intensity of the edge map is modulated to normalize values and emphasize specific regions. Equation 14 describes the modulation.

$$E \leftarrow 0.5 \cdot (0.5 - |T - 0.5|) \quad (14)$$

This equation centers edge values around 0.5 to reduce extreme variations and ensures that edges near the midpoint brightness of the image are given greater emphasis.

With the modulated edge map E, contrast is enhanced by amplifying the differences between pixel values and their surroundings. Each color channel $c(R, G\ B)$ is adjusted as in Equation 15.

$$P_c \leftarrow P_c + \delta \cdot E(15)$$

where $\delta$is a tunable parameter controlling the intensity of the enhancement, and $P_c$represents the pixel intensity in channel c.Increasing δ results in a sharper contrast, but excessive values lead to over-enhancement or artifacts.

2.3 Proposed Deep Learning Enhancement

Cycle GAN is a powerful DL framework for image-to-image translation without requiring paired datasets [18]. It translates images from one domain (e.g., low-quality images) to another domain (e.g., enhanced or high-quality images) while maintaining a cycle consistency that ensures the image's original features are preserved during the transformation [19]. This makes Cycle GAN particularly suitable for tasks like improving image color stabilization, saturation enrichment, contrast enhancement, and brightness adjustment. CycleGAN employs two main networks, Generator (G and F), which is responsible for translating images between domains X and Y and Discriminators **($\boldsymbol{D_X}$** and**$\boldsymbol{D_Y}$)**, to guarantee that the generated images resemble the real images in their respective target domains as demonstrated in Figure 3.

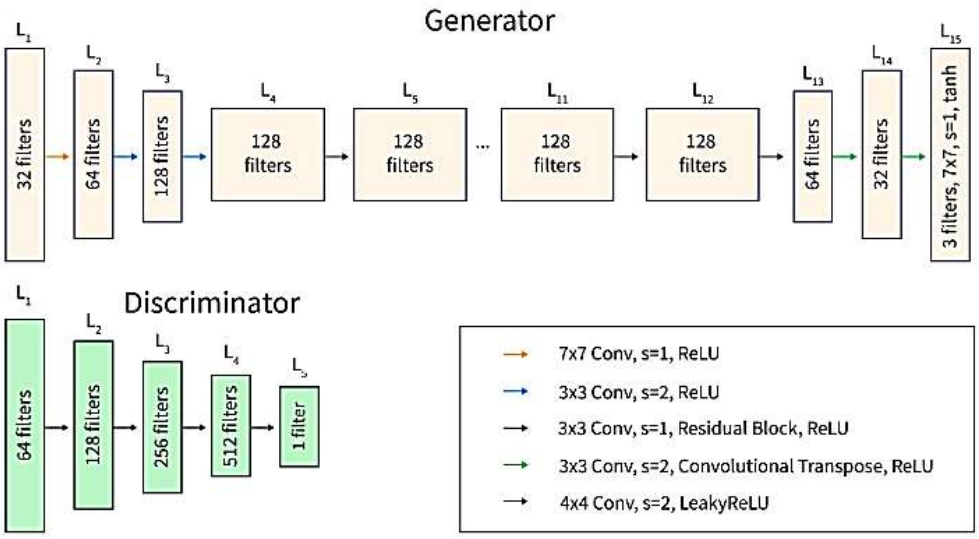

Figure 3. Cycle GAN Architecture

The adversarial loss drives the generators to create images that are indistinguishable from real images in the target domain. This is achieved by introducing a min-max game between the generators and discriminators. For a generator G translating images from domain X to Y, and a discriminator $\boldsymbol{D_Y}$ that evaluates images in domain Y, the adversarial loss is defined as in Equation 16.

$$\mathcal{L}_{GAN}(G, \boldsymbol{D_Y}, \mathrm{X}, \mathrm{Y}) = \mathbb{E}_{y \sim pdata(Y)}[log \boldsymbol{D_Y}(\boldsymbol{y})] + \mathbb{E}_{x \sim pdata(X)}[\log(1 - \boldsymbol{D_Y}(\boldsymbol{G}(\boldsymbol{x})))](16)$$

where$\boldsymbol{D_Y}(\boldsymbol{y})$ represents the probability that $\boldsymbol{D_Y}$ correctly identifies a real image y and $\boldsymbol{D_Y}(\boldsymbol{G}(\boldsymbol{x})$signifies the probability that $\boldsymbol{D_Y}$ correctly identifies the generated image $G(x)$ as fake.A similar adversarial loss can be defined for the generator F and discriminator $\boldsymbol{D_X}$, translating images from Y to X, as in Equation 17.

$$\mathcal{L}_{GAN}(F, \boldsymbol{D_X}, Y, X) = \mathbb{E}_{x\sim pdata(X)}[log\boldsymbol{D_X}(\boldsymbol{x})] + \mathbb{E}_{y\sim pdata(Y)}[log(1 - \boldsymbol{D_X}(\boldsymbol{F}(\boldsymbol{y})))](17)$$

The adversarial losses ensure that the generated images closely mimic the statistical characteristics of their target domains.

While adversarial loss ensures the quality of individual transformations, it doesn't guarantee that the content of the image remains consistent during the transformations $X \to Y \to X$ or $Y \to X \to Y$. The cycle consistency loss addresses this by enforcing that translating an image to the target domain and then back to its original domain yield a result close to the original image. Equation 18 expresses the cycle consistency loss.

$$\mathcal{L}_{cyc}(G, F) = \mathbb{E}_{x\sim pdata(X)}[\|F(G(x) - x\|_1] + \mathbb{E}_{y\sim pdata(Y)}[\|G(F(y) - y\|_1](18)$$

where$\|F(G(x) - x\|_1$ensures that after mapping $x \to y$ and $y \to x$, the image x remains unchanged and $\|G(F(y) - y\|_1$enforces the same for images in domain Y.

The total loss combines adversarial and cycle consistency losses to balance realism and content preservation, as in Equation 19.

$$\mathcal{L}(G, F, \boldsymbol{D_X}, \boldsymbol{D_Y}) = \mathcal{L}_{GAN}(G, \boldsymbol{D_Y}, \mathrm{X}, \mathrm{Y}) + \mathcal{L}_{GAN}(F, \boldsymbol{D_X}, Y, X) + \lambda\mathcal{L}_{cyc}(G, F)(19)$$

By employing Cycle GAN, natural color tones while enhancing saturation is ensured. Contrast and brightness adjustments benefit from Cycle GAN's ability to learn domain-specific transformations, improving visual quality. Additionally, entropy and sharpness are preserved through cycle consistency, which maintains image details and prevents degradation during translation. Cycle GAN's flexibility and its ability to operate on unpaired datasets make it ideal for real-world image enhancement applications without the need for extensive data curation. The whole process is detailed in Algorithm 1.

Algorithm 1. *Aerial Image Restoration using DLand Image Processing*

Input: *USC-SIPI Image Database*

Output: *Final Restored Image*

Begin

1. ***Load the input aerial image****:*
   - *Load the image from the dataset, typically in TIFF format.*
2. ***Color Stabilization***

❖ *Apply Color Stabilization*

- *For the image$P(x, y) = \{R(x, y), G(x, y), B(x, y)\}$, compute the mean brightness for each RGB channel μ_c,*

$$\mu_c = \frac{1}{N}\sum_{x,y} P_c(x, y)$$

- *Adjust each channel $P_c(x, y)$based on its mean brightness,*

$$P_c'(x,y) = \left(\frac{log(P_c(x,y))}{log\ (\mu_c)}\right)^{\psi_c}$$

- *Recombine the adjusted channels to form the color-stabilized image,*

$$P'(x,y) = \{\{P_R'(x,y), P_G'(x,y), P_B'(x,y)\}\}$$

3. *Saturation Enrichment*

❖ *Calculate saturation*

- *For each pixel, compute saturation S using,*

$$S = 1 - \frac{min(R,G,B)}{max(R,G,B)}$$

- *Normalize each channel,*

$$P_c' = \frac{P_c - min(P_c)}{max(P_c) - min(P_c)}$$

❖ *Adjust saturation*

- *Enhance the saturation by adjusting the minimum and maximum intensity values for each channel,* $\zeta \leftarrow (1-\lambda)\zeta, \psi \leftarrow \psi + (1-\lambda)$
- *Apply the scaling factor* μ *to update the saturation value* Ω.

$$\Omega = \mu \cdot (\psi - \zeta) + \zeta$$

$$\mu = \frac{\psi - \zeta}{\Omega}$$

- *Update the color channels with enhanced saturation.*

4. *Contrast Improvement*

❖ *Compute Brightness*

- *Compute the average brightness* T *as the mean intensity across the RGB channels*

$$T = \frac{1}{3}\sum_{C\in\{R,G,B\}} P_c$$

❖ *Edge Detection*

- *Apply the Laplacian kernel* K *to detect edges in the image.*

$$E = T \otimes K$$

- *Modulate the edge values*

$$E \leftarrow 0.5 \cdot (0.5 - |T - 0.5|)$$

❖ *Enhance Contrast*

- *Adjust the pixel intensities by adding the modulated edge map,*

$$P_c \leftarrow P_c + \delta \cdot E$$

5. *DL Enhancement with Cycle GAN*

❖ *Prepare Data for Cycle GAN*

- *Use the preprocessed image (with stabilized colors, enriched saturation, and improved contrast) as the input for Cycle GAN.*

❖ *Cycle GAN Architecture*

- *Generator* G*: Translates the image from the input domain* X *(low-quality image) to the target domain* Y *(high-quality image).*
- *Discriminator* $\boldsymbol{D_Y}$*: Distinguishes between real high-quality images and generated images.*
- *Generator* F*: Maps the enhanced image back from domain* Y *to domain* X.
- *Discriminator* $\boldsymbol{D_X}$*:Distinguishes between real low-quality images and generated images.*

❖ *Train Cycle GAN*

- *Adversarial Loss for Generators and Discriminators:*

$$\mathcal{L}_{GAN}(G, \boldsymbol{D_Y}, X, Y) = \mathbb{E}_{y\sim pdata(Y)}[log\boldsymbol{D_Y}(\boldsymbol{y})] + \mathbb{E}_{x\sim pdata(X)}[log(1 - \boldsymbol{D_Y}(\boldsymbol{G}(\boldsymbol{x})))]$$

$$\mathcal{L}_{GAN}(F, \boldsymbol{D_X}, Y, X) = \mathbb{E}_{x \sim pdata(X)}[log \boldsymbol{D_X}(\boldsymbol{x})] + \mathbb{E}_{y \sim pdata(Y)}[log(1 - \boldsymbol{D_X}(\boldsymbol{F}(\boldsymbol{y})))]$$

- *Cycle Consistency Loss*

$$\mathcal{L}_{cyc}(G, F) = \mathbb{E}_{x \sim pdata(X)}[\|F(G(x) - x\|_1] + \mathbb{E}_{y \sim pdata(Y)}[\|G(F(y) - y\|_1]$$

- *Total Loss*

$$\mathcal{L}(G, F, \boldsymbol{D_X}, \boldsymbol{D_Y}) = \mathcal{L}_{GAN}(G, \boldsymbol{D_Y}, X, Y) + \mathcal{L}_{GAN}(F, \boldsymbol{D_X}, Y, X) + \lambda \mathcal{L}_{cyc}(G, F)$$

❖ *Apply Cycle GAN:*
- *After training, apply the generators G and F to improve image quality, ensuring that the color, saturation, and contrast are enhanced while preserving important features.*

❖ *Obtain Final Restored Image*

6. Model Evaluation:
- *Evaluate:*

metrics=M. evaluate
- *Hyper parameter adjustment*

Save the Model
End

2.4 Hardware and Software Setup

The study employed a robust hardware and software setup for training and deploying the Cycle GAN model. The hardware configuration included an NVIDIA GeForce GTX 1080Ti GPU, an Intel Core i7 processor, and 32GB of RAM, enabling efficient processing of high-resolution images and smooth training. The Python-based Keras library, integrated with TensorFlow, was utilized as the DL framework, while Google Colab provided high computational power and an intuitive interface for development and experimentation. Hyper parameter tuning was performed to optimize performance and generalization, with key parameters including a learning rate of 0.0002 with linear decay starting at 100 epochs, a batch size of 4, a cycle consistency loss weight λ of 10, and training for 200 epochs. The model architecture employed 6 residual blocks for images, a PatchGAN discriminator with a (70×70) patch size, Adam optimizer, instance normalization in generators, batch normalization in discriminators, and a dropout rate of 0.5. This comprehensive setup ensured efficient training, high-quality output, and computational feasibility.

3. Results and Discussion

The studywas evaluated at various stages of the restoration pipeline. The observed changes in these parameters highlight the efficiency of the suggested restoration techniques in enhancing image quality.

PSNR measures the quality of the reconstructed image compared to the original. It is calculated using the MSE as in Equation 20.

$$PSNR = 10.log_{10}\left(\frac{MAX_I^2}{MSE}\right) \quad (20)$$

where $MAX_I$is the maximum pixel intensity value of the image. MSE is shown in Equation 21.

$$MSE = \frac{1}{MN}\sum_{i=1}^{M}\sum_{j=1}^{N}[I(i,j) - K(i,j)]^2 \quad (21)$$

where $I(i,j)$is the original image,$K(i,j)$ is the processed image and M, N are image dimensions.

SSIM evaluates the perceptual similarity between two images based on luminance, contrast, and structure, as shown in Equation 22.

$$SSIM(I,K) = \frac{(2_{\mu_I\mu_K}+C_1)(2_{\sigma_{IK}}+C_2)}{(\mu_I^2+\mu_K^2+C_1)(\sigma_I^2+\sigma_K^2+C_2)} \quad (22)$$

where$\mu_I\mu_K$,are the mean intensities of I and K respectively. σ_I^2,$\sigma_K^2$are the variance of I and K respectively, σ_{IK} is the covariance of I and K.C_1,C_2 are constants.

MAE quantifies the average absolute difference between the original and processed images, as given by Equation 23.

$$MAE = \frac{1}{MN}\sum_{i=1}^{M}\sum_{j=1}^{N}|I(i,j)| - K(i,j) \quad (23)$$

where $I(i,j)$ and $K(i,j)$ are the pixel values of the original and processed images, respectively. These metrics provide comprehensive evaluation criteria for assessing image quality in terms of pixel-level accuracy, perceptual similarity, and overall error minimization. Table 1 demonstrates the classification report of the suggested method.

Table 1. Classification report of the suggested model

Evaluation parameter	Values
PSNR	38.34
MSE	0.003
SSIM	0.9806
MAE	0.005

The evaluation metrics for the proposed image restoration and enhancement model demonstrate its exceptional performance and reliability. A PSNR of 38.34 dB signifies high-quality reconstruction, with minimal perceptual distortion between the restored and original images. The MSE of 0.003 further validates the model's accuracy, reflecting a negligible level of pixel-level error. Additionally, the SSIM of 0.9806 highlights near-perfect similarity in details, ensuring that the enhanced images retain critical visual attributes of the original. The MAE, at 0.005, indicates precise pixel-level enhancements with minimal absolute deviations. Collectively, these metrics confirm that the model effectively balances restoration accuracy and visual quality, making it highly suitable for tasks requiring both fidelity and detail preservation.

Table 2 details the remarks of these parameters for images at various phases of the process of restoration. It is observed that simultaneous modifications occur in the parameter values at various phases of the restoration process.

Table 2. Parameter observations across different phases of the image restoration process

Parameters	**Input image**			
	Input	**Saturation Enriched**	**Contrast Improved**	**Color Stabilized**
Saturation	0.340	0.320	0.360	0.290
Entropy	6.200	6.900	7.100	6.800
Contrast	0.015	0.035	0.045	0.025
Brightness	0.600	0.520	0.550	0.500

This table demonstrates parameter improvements across different phases, reflecting the high quality of restoration and enhancement as evidenced by the high PSNR, SSIM, and low MAE and MSE values in Table 1.

It is important to note that the restoration process aims to enhance various image characteristics, such as saturation, contrast, entropy, and brightness, which are critical for improving image quality. The following Figures 4 to 7 illustrate how these parameters evolve during the restoration process.

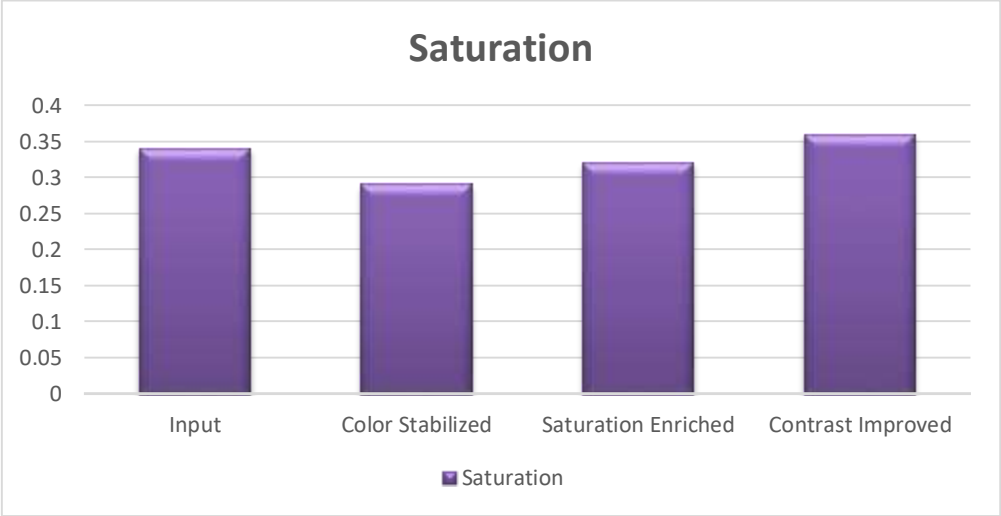

Figure 4. Comparison of saturation

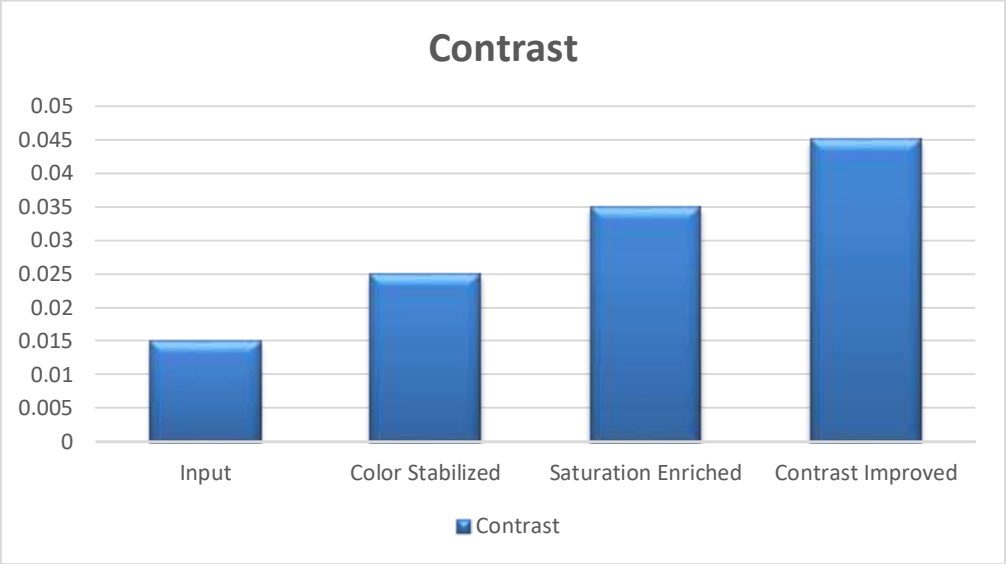

Figure 5. Comparison of contrast

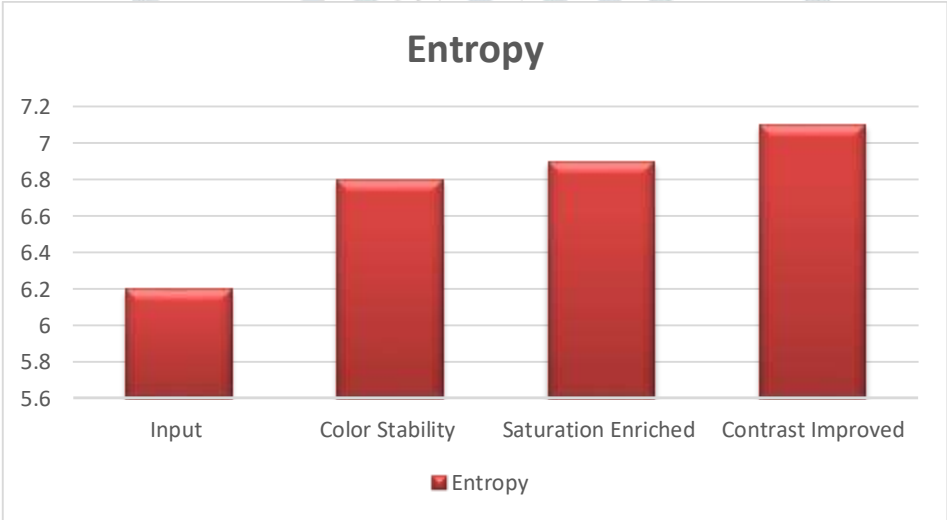

Figure 6. Comparison of entropy

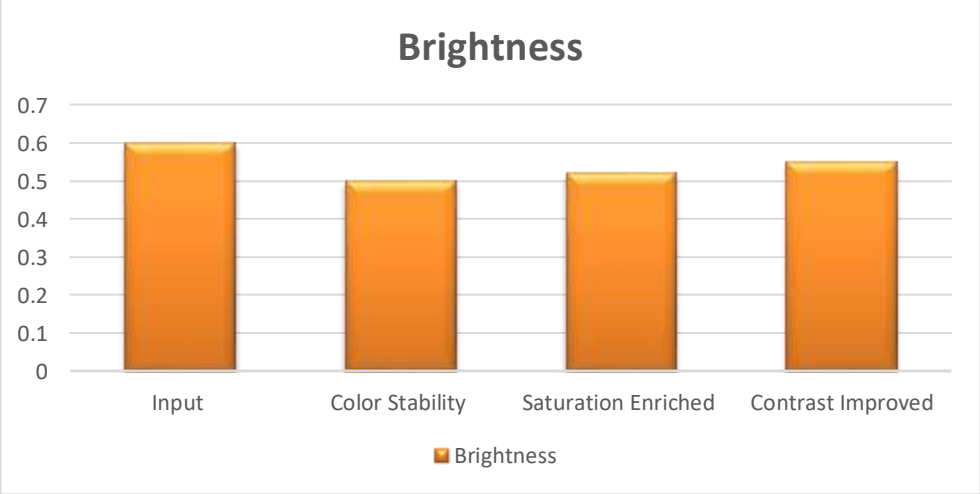

Figure 7. Comparison of brightness

The proposed digital image processing technique significantly enhances aerial image restoration by adjusting key parameters such as saturation, contrast, entropy, and brightness. While saturation is reduced initially, it is carefully managed to avoid over-saturation, ensuring the image retains natural color representation. Contrast improvement is evident through a gradual increase, which enhances the differentiation between light and dark areas, making finer details in the aerial imagery more visible and aiding in precise analysis. The increase in entropy indicates that the image becomes more detailed and sharper, preserving fine textures and structures critical for applications like environmental monitoring and urban planning. Finally, the slight decrease in brightness followed by a controlled increase ensures a balanced dynamic range, preventing areas from being too dark or bright. This technique, therefore, not only improves visual quality but also preserves important features, making it highly effective for aerial image restoration and analysis.

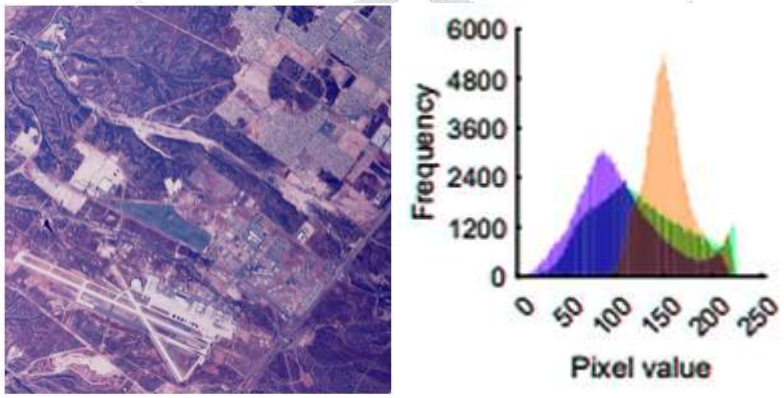

(a) (b)

Figure 8. (a) Input image (b) histogram of input image

Figure 8 demonstrates the sample input image and its histogram and Figure 9 demonstrates the predicted output of the proposed model after digital image processing techniques.

(a) (b)

(c) (d)

Figure 9. Predicted output of image processing techniques (a) input image (b) image after color stabilization (c) image after saturation enrichment (d) restored image.

Table 3. Performance comparison of the suggested model with existing methods

Model	PSNR	SSIM
Deep Neural Network [8]	37.42	0.9743
LAE-GAN [9]	18.94	0.6223
RFSUNET [10]	32.89	0.9436
DWDDSAE [12]	38.08	0.8831
RT-CBAM [16]	28.45	0.942
Proposed Model	**38.34**	**0.9806**

The performance of the proposed model is compared with existing model as detailed in Table 3.The proposed CycleGAN-based model demonstrated superior performance in image restoration tasks compared to state-of-the-art techniques. With a PSNR of 38.34 and an SSIM of 0.9806, it outperformed models like DWDDSAE (PSNR: 38.08, SSIM: 0.8831) and RFSUNET (PSNR: 32.89, SSIM: 0.9436) by achieving higher structural similarity and peak signal-to-noise ratio. Unlike traditional approaches that excel in specific areas but struggle with generalizability, the Cycle GAN model effectively handled complex degradations, preserving intricate details and minimizing noise. Its generative adversarial architecture enabled robust mapping of features between degraded and restored images, ensuring both global consistency and local refinement. Additionally, the Cycle GAN approach addressed limitations in sharpness and color restoration that constrained models like LAE-GAN and RT-CBAM, while maintaining

computational efficiency and adaptability to diverse degradation types. These attributes make the proposed model a comprehensive solution for high-quality image restoration across various applications.

4. Conclusion

This study presents an advanced approach to aerial image restoration using a combination of digital image processing techniques and deep learning, specifically Cycle GAN. The proposed methodology effectively addresses common challenges in aerial imagery, such as poor contrast, color imbalances, and saturation issues. By integrating color stabilization, saturation enrichment, and contrast improvement, followed by DL enhancement through Cycle GAN, the model significantly enhances image quality, ensuring high fidelity and detail retention. The evaluation metrics, including a PSNR of 38.34 dB, SSIM of 0.9806, and MAE of 0.005, demonstrate the model's superior performance in comparison to existing methods. These results indicate the model's ability to preserve structural integrity while reducing perceptual distortion and pixel-level error. Moreover, the Cycle GAN framework's adaptability to unpaired data and its robust performance across various degradation scenarios make it an ideal solution for real-world aerial image restoration. This work contributes to the field of image processing by offering a comprehensive, high-performance model that can be applied to a wide range of imaging tasks, ensuring more accurate and usable aerial imagery for critical decision-making processes.

References

1. Katsaggelos, A. K. (2012). *Digital image restoration*. Springer Publishing Company, Incorporated.
2. Lagendijk, R. L., & Biemond, J. (2009). Basic methods for image restoration and identification. In The essential guide to image processing (pp. 323-348). Academic Press.
3. Zhang, K., Zuo, W., Gu, S., & Zhang, L. (2017). Learning deep CNN denoiser prior for image restoration. In *Proceedings of the IEEE conference on computer vision and pattern recognition* (pp. 3929-3938).
4. Mohsan, S. A. H., Othman, N. Q. H., Li, Y., Alsharif, M. H., & Khan, M. A. (2023). Unmanned aerial vehicles (UAVs): Practical aspects, applications, open challenges, security issues, and future trends. *Intelligent Service Robotics*, *16*(1), 109-137.
5. Bhabatosh, C. (2011). *Digital image processing and analysis*. PHI Learning Pvt. Ltd..
6. Pashaei, M., Starek, M. J., Kamangir, H., & Berryhill, J. (2020). Deep learning-based single image super-resolution: an investigation for dense scene reconstruction with UAS photogrammetry. *Remote Sensing*, *12*(11), 1757.
7. Chen, Z., Wu, H., Li, W., & Wang, J. (2023, June). Enhanced Deconvolution and Denoise Method for Scattering Image Restoration. In *Photonics* (Vol. 10, No. 7, p. 751). MDPI.
8. Dutta, S., Basarab, A., Georgeot, B., & Kouamé, D. (2024). DIVA: Deep unfolded network from quantum interactive patches for image restoration. *Pattern Recognition*, 110676.
9. Nam, S. H., Kim, Y. H., Choi, J., Hong, S. B., Owais, M., & Park, K. R. (2021). Lae-gan-based face image restoration for low-light age estimation. *Mathematics*, *9*(18), 2329.

10. Jung, H. M., Kim, B. H., & Kim, M. Y. (2020). Residual forward-subtracted U-shaped network for dynamic and static image restoration. *IEEE Access*, *8*, 145401-145412.
11. Zhao, J., Kumar, A., Banoth, B. N., Marathi, B., Rajalakshmi, P., Rewald, B., ... & Guo, W. (2022). Deep-learning-based multispectral image reconstruction from single natural color RGB image—Enhancing UAV-based phenotyping. *Remote Sensing*, *14*(5), 1272.
12. Kiruthika, S., Priscilla, G. M., Vijendran, A. S., Batumalay, M., & Xu, Z. (2024). Deep Wiener Deconvolution Denoising Sparse Autoencoder Model for Pre-processing High-resolution Satellite Images. *Journal of Applied Data Sciences*, *5*(3), 1386-1398.
13. Nehete, H., Monga, A., Kaushik, P., & Kaushik, B. K. (2024). Fourier Prior-Based Two-Stage Architecture for Image Restoration. In *Proceedings of the IEEE/CVF Conference on Computer Vision and Pattern Recognition* (pp. 6014-6023).
14. Yuan, Y., Gang, G. J., & Stayman, J. W. (2024). DLCT Image Restoration using System Blur and Noise Models. *arXiv preprint arXiv:2407.14983*.
15. Guo, H., Li, J., Dai, T., Ouyang, Z., Ren, X., & Xia, S. T. (2025). Mambair: A simple baseline for image restoration with state-space model. In *European Conference on Computer Vision* (pp. 222-241). Springer, Cham.
16. Ye, R., Qian, Y., & Huang, X. (2024). RT-CBAM: Refined Transformer Combined with Convolutional Block Attention Module for Underwater Image Restoration. *Sensors*, *24*(18), 5893.
17. https://www.kaggle.com/datasets/luffyluffyluffy/the-uscsipi-image-database/data
18. Wang, T., & Lin, Y. (2024). CycleGAN with better cycles. *arXiv preprint arXiv:2408.15374*.
19. Rajagopal, B. G., Kumar, M., Alshehri, A. H., Alanazi, F., Deifalla, A. F., Yosri, A. M., & Azam, A. (2023). A hybrid Cycle GAN-based lightweight road perception pipeline for road dataset generation for Urban mobility. *Plos one*, *18*(11), e0293978.